https://doi.org/10.5194/angeo-2020-78
Preprint. Discussion started: 8 December 2020

Annales Geophysicae Discussions

Microbarom radiation and propagation model assessment using infrasound recordings: a vespagram-based approach

Ekaterina Vorobeva[1,2], Marine De Carlo[3,4], Alexis Le Pichon[3], Patrick Joseph Espy[1], and Sven Peter Näsholm[2,5]

[1]Department of Physics, Norwegian University of Science and Technology, Trondheim, Norway
[2]NORSAR, Kjeller, Norway
[3]CEA, DAM, DIF, F-91297, Arpajon, France
[4]Univ. Brest, CNRS, IRD, Ifremer, Laboratoire d'Océanographie Physique et Spatiale (LOPS), IUEM, Brest, France
[5]Department of Informatics, University of Oslo, Oslo, Norway

Correspondence: Ekaterina Vorobeva (ekaterina.vorobeva@ntnu.no)

Abstract. This study investigates the use of a vespagram-based approach as a tool for multi-directional comparison between simulated microbarom soundscapes and infrasound data recorded at ground-based array stations. Data recorded at the IS37 station in northern Norway during 2014 – 2019 have been processed to generate vespagrams (velocity spectral analysis) for five frequency bands between 0.1 and 0.6 Hz. The back-azimuth resolution between vespagrams and a microbarom model is harmonized by smoothing the modelled soundscapes along the back-azimuth axis with a kernel corresponding to the frequency-dependent array resolution. An estimate of similarity between the output of a microbarom radiation and propagation model and infrasound observations is then generated based on the image processing approach of mean-square difference. The analysis revealed that vespagrams can monitor seasonal variations in the microbarom azimuth distribution, amplitude, and frequency, as well as changes during sudden stratospheric warming. The vespagram-based approach is computationally inexpensive, can uncover microbarom source variability, and has potential for near-real-time stratospheric diagnostics and atmospheric model assessment. Keywords: infrasound, vespa, microbaroms, array signal processing, stratosphere, atmospheric models

1 Introduction

Microbaroms are infrasound waves with frequencies typically between 0.1 and 0.6 Hz generated by non-linear interaction between counter-propagating ocean waves. Because of the low frequencies, microbaroms can penetrate the middle atmosphere and return back to ground at long ranges. Hence there is potential to exploit this source to probe the dynamics of this altitude range, where the representation of the atmospheric dynamics in model products is often poorly constrained (Polavarapu et al., 2005; Rienecker et al., 2011; Smith, 2012; Amezcua et al., 2020).

https://doi.org/10.5194/angeo-2020-78
Preprint. Discussion started: 8 December 2020

The term "microbarom" was established by Benioff and Gutenberg (1939) who described quasi-continuous pressure fluctuations with periods of $0.5-5$ s recorded by two electromagnetic barographs installed by the Seismological Laboratory, California Institute of Technology, Pasadena, USA. Following Benioff and Gutenberg (1939), several microbarom studies were performed by scientists around the globe. Joint observation of microbaroms and microseisms (quasi-continuous fluctuations of ground displacement generated by the ocean waves) in California, USA (Gutenberg and Benioff, 1941), Christchurch, New Zealand (Baird and Banwell, 1940), Fribourg, Switzerland (Saxer, 1945, 1954; Dessauer et al., 1951) and New York, USA (Donn and Posmentier, 1967) demonstrated that the microbarom signals originate from the ocean.

Thereafter, efforts were made to develop theories to explain the physical mechanisms of microbarom generation (Brekhovskikh et al., 1973; Waxler et al., 2007). A recent model proposed by De Carlo et al. (2020) unifies aforementioned theories of microbarom generation, taking into consideration both finite ocean-depth and the source radiation dependence on elevation and azimuth angles. This model can predict location and intensity of the source when coupled with an ocean wave spectrum model. However, for comparison with infrasonic observations at distant ground-based stations, it is necessary to consider the influence of the atmospheric structure on the microbarom propagation and ducting. This can, for example, be estimated using a semi-empirical range-dependent attenuation model in a horizontally homogeneous atmosphere (Le Pichon et al., 2012), or wave propagation simulation using 3-D ray tracing (Smets and Evers, 2014). Details on our suggested vespagram-based comparison approach to microbaroms modeled by a state-of-the-art microbarom radiation theory (De Carlo et al., 2020) are presented in Sect. 2.2.

In array signal processing, velocity spectral analysis (vespa) is an approach which analyzes recorded signals in terms of signal power as a function of time (Davies et al., 1971). The power is evaluated either at a fixed slowness, i.e. a constant apparent velocity with varying back-azimuth — corresponding to a circle in the slowness space — or at a fixed back-azimuth with varying apparent velocity — corresponding to a line in slowness space. The vespa power estimate can therefore be visualized as an image, called vespagram, with time on one axis and either back-azimuth (for a fixed apparent velocity) or apparent velocity (for a fixed back-azimuth) as the other axis.

In this study, vespagrams estimated from infrasound array data for a fixed apparent velocity of 350 m/s corresponding to the stratospheric arrival regime are used. For a given frequency band, such vespagrams can straightforwardly be compared to microbarom soundscapes modeled for a station location after applying a smoothing kernel which harmonizes the resolution given by the array response function main lobe with the resolution of the microbarom model output. Both the vespagram and the microbarom model provide power estimates as function of time and back-azimuth which can be displayed as an image, and we utilize an image comparison approach based on mean-square difference for benchmarking. The study considers 6 consecutive years of infrasound observations between 2014 and 2019 at a ground-based infrasound array located at Bardufoss, Norway (69.07° N, 18.61° E), denoted IS37 or I37NO (Fyen et al., 2014). See Sect. 2.1 for details on the station configuration, data, and the processing applied in this study.

The proposed vespagram-based approach is computationally low-cost and can monitor microbarom source variability over a year (Sect. 3.1) as well as detect changes during extreme atmospheric events such as sudden stratospheric warmings (Sect. 3.2). It might be further refined for applications such as near-real time diagnostics of ocean wave and atmospheric models, as well as for long-term assessment of model product uncertainties, particularly when applied to data from a global network of infrasound stations. A key aspect of this approach is that benchmarking between model and infrasound vespagrams considers all back-azimuth directions rather than just the direction of the dominant microbarom source, as done in several previous studies (Garcés et al., 2004; Hupe et al., 2019; De Carlo et al., 2019; Smirnov et al., 2020; De Carlo et al., 2020). The microbarom soundscape at a station is typically a sum of components stemming from a wide spatial distribution of ocean regions, and recently den Ouden et al. (2020) demonstrated that an iterative decomposition of the array spatial covariance matrix using the CLEAN algorithm (Högbom, 1974) can be exploited to resolve the back-azimuth and trace velocity of the most coherent wave front arrivals.

A long-term ambition is to exploit microbarom infrasound datasets to enhance the representation of stratospheric dynamics in atmospheric model products and hence increase the accuracy of both medium-range weather forecasting and sub-seasonal climate modeling (Büeler et al., 2020; Dorrington et al., 2020; Domeisen et al., 2020a, b). In addition to prospective numerical weather prediction improvements, the suggested vespagram-based approach may be applied in multi-technology studies of atmospheric dynamics, for example initiatives building on the Atmospheric dynamics Research InfraStructure in Europe (ARISE) projects (Blanc et al., 2018, 2019). These aim at harvesting from synergies between ground-based infrasound observations, radar and lidar systems, as well as airglow and satellite observations to monitoring the middle atmosphere (Chunchuzov et al., 2015; Le Pichon et al., 2015; Blanc et al., 2018; Hupe et al., 2019; Smets et al., 2019; Hibbins et al., 2019; Assink et al., 2019; Le Pichon et al., 2019).

The study is organized as follows. The data and method are described in Sect. 2; the main results are presented in Sect. 3 followed by discussion in Sect. 4.

2 Materials and Methods

2.1 Infrasound dataset and signal processing

The infrasound array denoted IS37 or I37NO was initially planned to be co-located with the ARCES seismic array in Karasjok, Norway, (69.5° N, 25.5° E) as part of the International Monitoring System (IMS) which verifies compliance with the Comprehensive Nuclear-Test-Ban Treaty (CTBT) (Dahlman et al., 2009; Marty, 2019). Instead, the station was installed at a location more favourable for infrasound monitoring in Bardufoss, Norway (69.07° N, 18.61° E), and equipped with ten MB3 type (MB2005 prior to 2016) microbarometers over an aperture of 2 km (Figure 1a) (Fyen et al., 2014). The station was certified by the CTBT Organization on 19 December 2013 and is operated by NORSAR, Kjeller, Norway. Besides being included in the IMS, IS37 is also part of a regional network of European infrasound stations (Gibbons et al., 2007, 2015, 2019) that resolves significantly smaller events than the global IMS network (Le Pichon et al., 2008). In the framework of the regional network, data from IS37 has been used for multi-station studies characterizing European infrasound sources (e.g., Pilger et al., 2018).

The IS37 station routinely detects microbaroms within $0.1-0.6$ Hz originating from the North Atlantic, the Barents Sea, and beyond. An analytical expression for a plane-wave front incident on the IS37 array was used to characterize the array's integrated, frequency-dependent response in 0.1 Hz wide frequency bands from 0.1 to 0.6 Hz. The wave front was representative

https://doi.org/10.5194/angeo-2020-78
Preprint. Discussion started: 8 December 2020

Annales Geophysicae
Discussions
Open Access

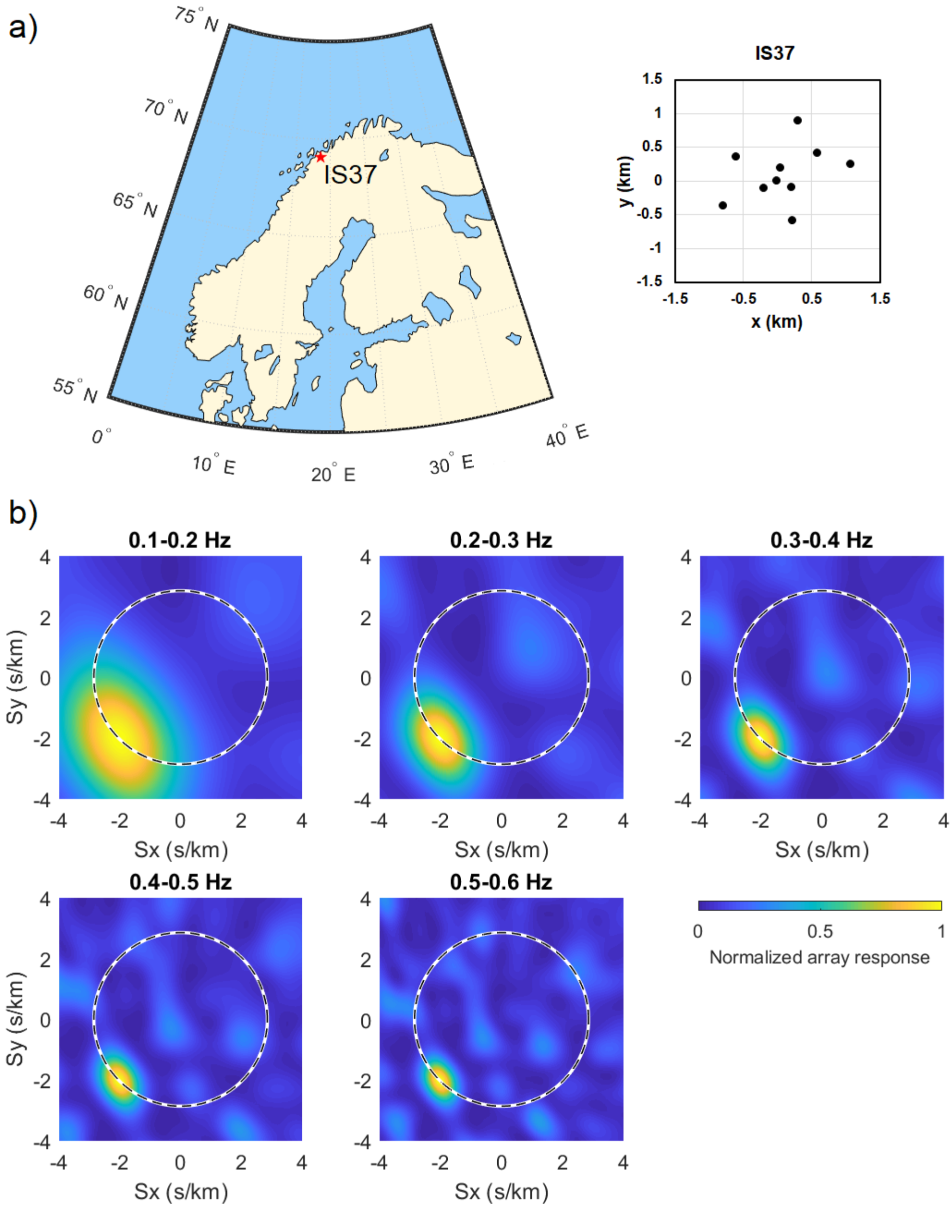

Figure 1. a) The IS37 infrasound array location and geometry. b) Integrated steered array response for 0.1 Hz wide frequency bands assuming a plane wave impinging at 225° back-azimuth and 350 m/s apparent velocity (indicated with a dashed circle).

of a microbarom signal from the Atlantic Ocean, with a back-azimuth of 225° and a 350 m/s apparent velocity typical of the stratospheric regime (Garcés et al., 1998; Whitaker and Mutschlecner, 2008; Nippress et al., 2014; Lonzaga, 2015). The base resolution of the array was taken to be the 1-sigma beam width of the Gaussian fitted to the array response at a constant velocity

https://doi.org/10.5194/angeo-2020-78
Preprint. Discussion started: 8 December 2020

Annales Geophysicae
Discussions

of 350 m/s (dashed line in Figure 1b) for each frequency band. The resulting resolution was found to be: $35°$, $23°$, $16°$, $13°$ and $10°$ for $0.1-0.2$ Hz, $0.2-0.3$ Hz, $0.3-0.4$ Hz, $0.4-0.5$ Hz and $0.5-0.6$ Hz band, respectively. It should be noted that this estimate is based on the homogeneous medium plane-wave time-delays between the array elements only and does not take into account meteorological conditions at the station, noise, or other coherence loss mechanisms that may result in a wider beam width.

In array signal processing, separating coherent from incoherent parts of the recorded signal, as well as the separation between different simultaneous arrivals are important concepts. When analyzing the wavefield in terms of a given horizontal slowness vector (e.g., described in terms of apparent velocity and back-azimuth), delay-and-sum beamforming (Ingate et al., 1985) is usually applied in combination with the underlying plane-wave model assumption. This method applies time-delays to the array sensor traces to focus on wave fronts arriving with a specific horizontal apparent velocity and a specific back-azimuth direction, hence amplifying wavefield components with the horizontal slowness of interest, while suppressing other components. However, the slowness vector models are not always accurate (Gibbons et al., 2020). In particular, the actual shape of the wave front arriving at infrasound arrays may differ from a theoretical plane-wave due to meteorological conditions and turbulence at the station, which make the underlying assumption of a locally homogeneous effective sound speed invalid. In this case, the beamforming is less efficient and the reduced array gain results in lower stack amplitude and signal distortion (Rost and Thomas, 2002).

To determine an unknown slowness vector component and to study the spatial structure of the wavefield over time, one can use the vespa (velocity spectral analysis) processing. This not only enhances the signal as the beamforming does, but also allows one to determine either the direction or apparent velocity of incoming signal. The vespa method estimates the power of the signal either for a fixed apparent velocity with varying back-azimuth or for a fixed back-azimuth with varying apparent velocity. The result of the vespa processing is usually presented as an image displaying the power of incoming signal as a function of time and back-azimuth (or apparent velocity) called vespagram. Despite that vespa is a widely applied in seismological array data studies (e.g., Davies et al., 1971; Kanasewich et al., 1973; Muirhead and Datt, 1976; McFadden et al., 1986), it has not previously been exploited in peer-reviewed microbarom infrasound studies.

The vespa processing procedure described below is applied to each analyzed time window and frequency band:

1) For each sensor n of an array, we extract signal recording $x_n(t)$ that corresponds to the time window of interest. The analysis here is done for an 1h moving time window, evaluated every 30 min. In general, the time series recorded at sensor n at the location $\boldsymbol{r}_n$ can be written as

$$x_n(t) = y(t - \boldsymbol{r}_n \cdot \boldsymbol{s}_{\text{hor}}), \tag{1}$$

where $y(t)$ represents a plane wave front signal, and $\boldsymbol{s}_{\text{hor}}$ is the horizontal component of the slowness vector.

2) Remove the mean.

3) Apply a Butterworth bandpass filter to recordings. Calculations are performed for five equally spaced frequency bands that are within the microbarom frequency range (see Figure 1b).

https://doi.org/10.5194/angeo-2020-78
Preprint. Discussion started: 8 December 2020

4) Beam traces or delay-and-sum traces of an array with N sensors are computed as

$$b(t) = \frac{1}{N}\sum_{n=1}^{N} x_n(t + \boldsymbol{r}_n \cdot \boldsymbol{s}_{\text{hor}}). \tag{2}$$

In this study, classical linear vespa processing (Davies et al., 1971) is applied where the noise suppression is proportional to square root of N (Rost and Thomas, 2002). A beam is generated at each 1° in back-azimuth, for the fixed apparent velocity of 350 m/s, which is within stratospheric arrival regime (Garcés et al., 1998; Whitaker and Mutschlecner, 2008; Nippress et al., 2014; Lonzaga, 2015). That allows to estimate signals coming from all directions but from approximately the same height corresponding to stratospheric altitudes.

5) Calculate mean squared pressure (power) of each beam to get an estimate of incoming signal strength as a function of back-azimuth and time.

Steps (1) – (5) are applied to all analyzed years of data.

2.2 Microbarom source and propagation modeling

In this section we summarize the approach applied to get directional spectrum of microbarom soundscape as a function of time. The procedure is as follows.

1. *Ocean wave model:* The WAVEWATCH III ® (The WW3 Development Group, 2016) code gives an estimate of the generation and variation of the wave spectrum based on surface winds. The interaction of counter propagating waves is calculated from these wave spectra as described in (Ardhuin et al., 2011). Studies on microseisms (Landès et al., 2014; Hillers et al., 2012) have demonstrated the limitations of a model that does not account for coastal reflection. Therefore, in this study the parametrization used to run the WW3 model accounts for fixed reflection coefficients of 10 % for the continents, 20 % for the islands and 40 % for ice sheets (Ardhuin et al., 2011) and provides the spectral density of equivalent surface pressure forcing microbaroms on a global scale with 0.5° latitudinal - longitudinal resolution and a 3-hours time-step (corresponding to the variable 'p2l' available at ftp://ftp.ifremer.fr/ifremer/ww3/HINDCAST/SISMO/).

2. *Microbarom source model:* A microbarom source model is basically a model transforming ocean wave model output into acoustic radiation spectrum in the atmosphere. Here, calculations are based on the model of De Carlo et al. (2020), taking into consideration both finite ocean-depth and a source radiation depending on elevation and azimuth angles. This microbarom model allows prediction of the location and intensity of the microbarom sources when applied to the Hasselmann integral. The Hasselmann integral is derived from the output of the wave model and establishes a relationship between the source spectrum and the spectral densities of counter propagating waves for a given frequency (Hasselmann, 1963). The output of this step is an acoustic spectrum for each cell of the wave model.

3. *Microbarom propagation in the atmosphere:* A semi-empirical attenuation law (Le Pichon et al., 2012) is applied to the microbarom spectra obtained through the previous step. This law accounts for the distance between the source and the

https://doi.org/10.5194/angeo-2020-78
Preprint. Discussion started: 8 December 2020

station as well as for frequency but assumes horizontally homogeneous atmosphere. The atmospheric conditions are considered as the $V_{\text{eff-ratio}}$, the ratio of effective sound speed in the propagation direction between the stratosphere at 50 km and ground. Atmospheric wind and temperature needed to assess $V_{\text{eff-ratio}}$ are derived from the European Center for Medium range Weather Forecasting (ECMWF) models (http://www.ecmwf.int). $V_{\text{eff-ratio}}$ is calculated from the atmospheric profile at the station in order to assess the possibility of wave front arrival from different directions.

4. *Summation of sources:* At this step, for each cell of the wave model, an acoustic spectrum is generated and attenuated to reflect what would be seen by the station. To obtain the directional spectrum at the station, all attenuated spectra from model cells within a 1° azimuth band and less than 5000 km away from the station are summed. The distance limitation comes from the attenuation law definition. Although this attenuation law is widely used for propagation over very long distances (Smirnov et al., 2020; Pilger et al., 2019; Hupe et al., 2019; De Carlo et al., 2019, 2020), it was designed for distances up to 3000 km only. For IS37, as the main sources are quite close to the station, expanding this attenuation law all around a great circle can lead to misrepresentation of remote sources. However, in our case the limit can still be expanded to 5000 km (private communication with M. De Carlo). Thus, all sources that are more than 5000 km away from the station are excluded from the study.

After applying these steps, and integrating over the frequency bands, we get an estimate of microbarom amplitude as function of time and back-azimuth, just as vespagrams. However, vespagrams cannot be directly compared to the modelled microbarom soundscapes since the latter do not take into account the frequency-dependent resolution of array. Therefore, we smooth the modelled microbarom soundscapes by convolving with a Gaussian kernel at each time step taking into account cyclical nature of back-azimuth when smoothing near $360°/0°$. Kernels are normalized to have sum of 1, and their standard deviations (width) decrease with frequency (see Sect. 2.1).

3 Results

3.1 Comparison for full seasons

Figures 2 and 3 present benchmarking microbarom model and vespa processing images (vespagrams) for two frequency bands, namely $0.1-0.2$ Hz and $0.5-0.6$, for 2016. Panel a) in Figures 2 and 3 show the seasonal behavior of the dominant signal amplitude over a year. Enhanced ocean source activity during winter is accompanied with eastward stratospheric wind favorable for ducting infrasound over long distances (Le Pichon et al., 2006). This results in a peak of microbarom pressure amplitude both in model and vespagrams regardless of frequency band. As seen from panels b) – d) in Figures 2 and 3, the microbarom radiation model by De Carlo et al. (2020) accompanied with semi-empirical wave attenuation law accurately reproduces infrasound detections. This is especially true after applying smoothing, which results in better agreement between direction of the dominant signal in model and vespagrams (Figure 4).

Due to the strong seasonal variability of microbarom amplitude it is difficult to compare the direction of winter to summer detections on an absolute amplitude scale. Thus, we normalize panels b) – d) in Figures 2 and 3 at each time step (panels e) – j),

https://doi.org/10.5194/angeo-2020-78
Preprint. Discussion started: 8 December 2020

Annales Geophysicae Discussions Open Access EGU

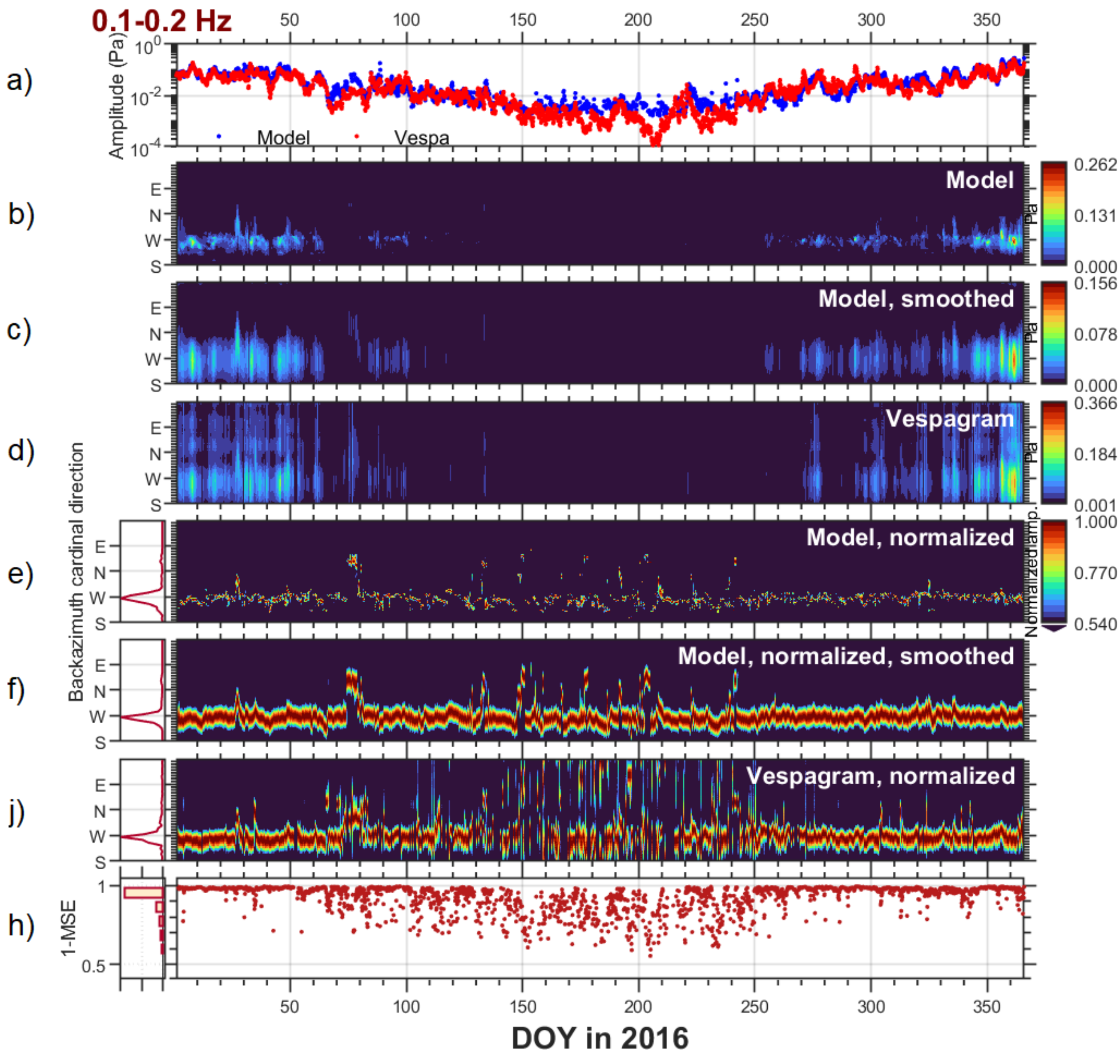

Figure 2. Benchmarking microbarom model and infrasound vespagram for 0.1 – 0.2 Hz in 2016 for the IS37 station. a) amplitude of dominant signal (blue – vespa processing, red – model); b) microbarom model output; c) model output after smoothing (Sect. 2.2); d) infrasound vespagram (Sect. 2.1); e) – j) (right) same as panels 2 – 4 but after normalization at each time step; e) – j) (left) normalized directional distribution of dominant signal (10° bins); h) similarity score between panels 6 and 7 (right) and its normalized distribution (left). Panels b) – j) are visualized using the Turbo colormap (Mikhailov, 2019).

https://doi.org/10.5194/angeo-2020-78
Preprint. Discussion started: 8 December 2020

Annales Geophysicae
Discussions
Open Access

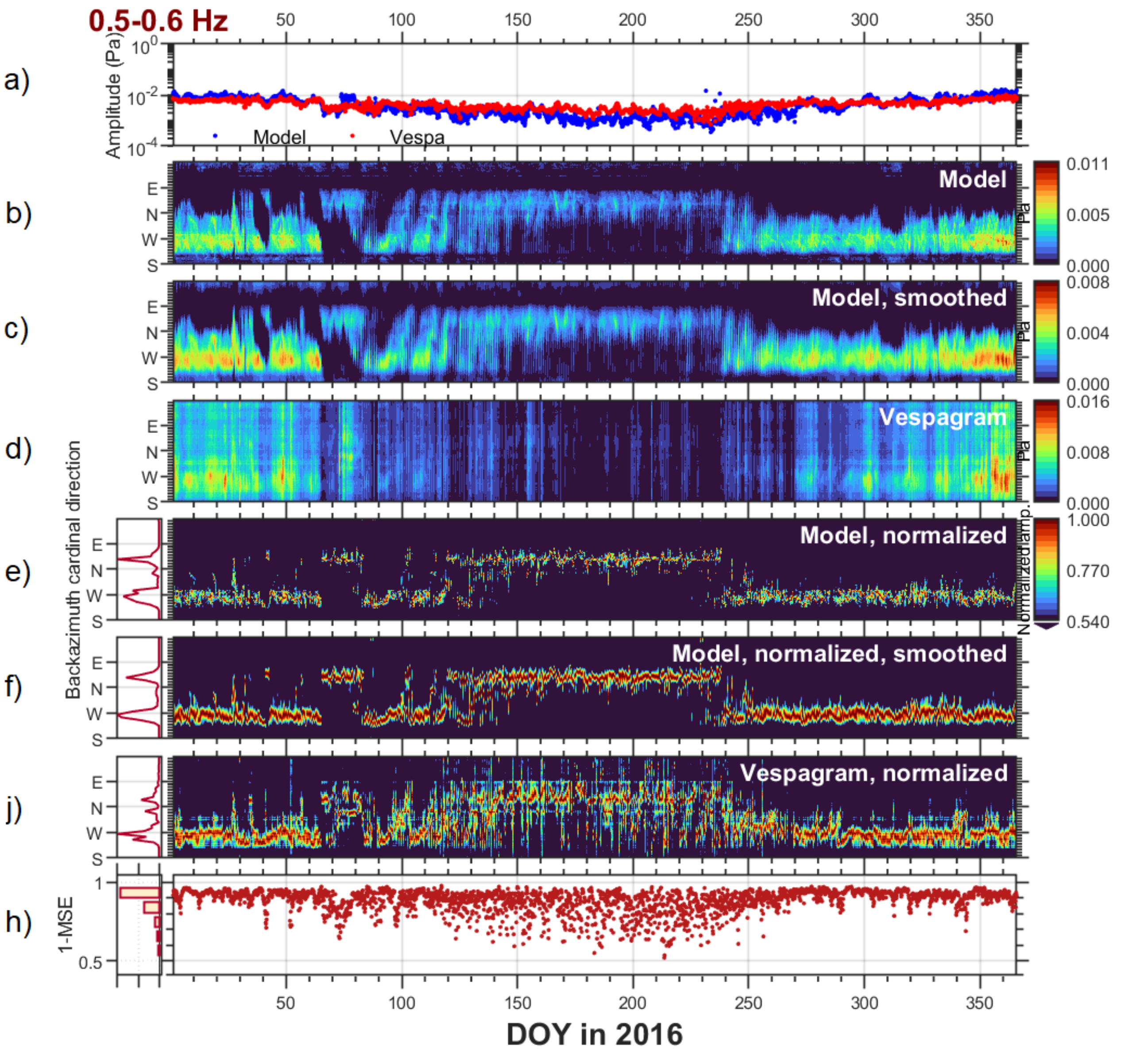

Figure 3. Same as Figure 2 but for 0.5 – 0.6 Hz.

right) and estimate directional distribution of dominant signal in 10° bins (panels e) – j), left). For a frequency band of 0.1 – 0.2 Hz the North Atlantic is the dominant source direction throughout the year (Figure 2). Going to higher frequencies, there is a pronounced change in the dominant direction of the source from the Atlantic in winter to the Barents Sea in summer (Figure 3). This is associated with the change of wind direction in the stratosphere from eastward to westward. Analysis of 6 years

https://doi.org/10.5194/angeo-2020-78
Preprint. Discussion started: 8 December 2020

Annales Geophysicae
Discussions
Open Access
EGU

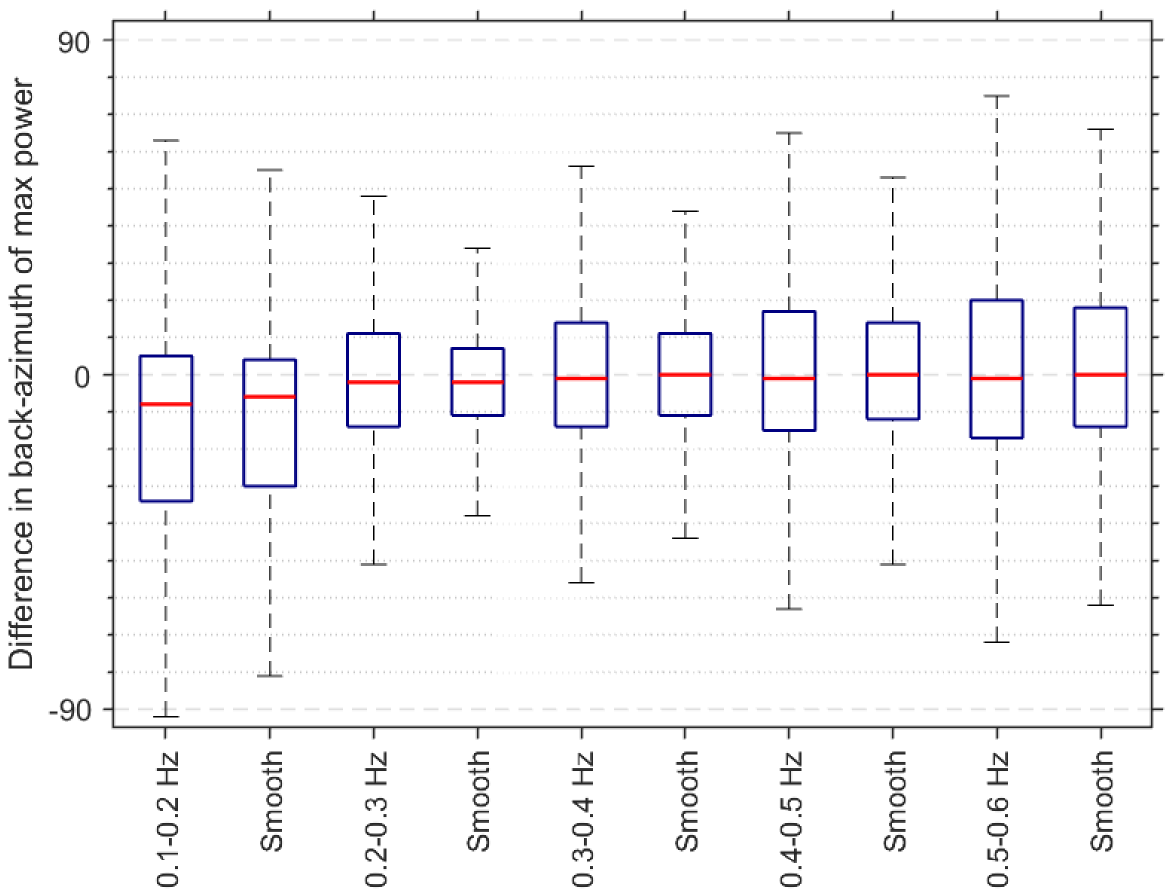

Figure 4. A difference in direction of maximum power between i) model and vespagram (indicated with a frequency band name in x-axis) and ii) smoothed model and vespagram (indicated as "smooth" in x-axis) over 6 years of data at the IS37 station. Red lines present median, blue boxes indicate a range between 25 and 75 percentiles, whiskers correspond to $\pm 3\sigma$.

https://doi.org/10.5194/angeo-2020-78
Preprint. Discussion started: 8 December 2020

dataset in terms of the dominant source direction indicates three prevailing microbarom source regions associated with the North Atlantic, the Greenland Sea, and the Barents Sea. These appear at the vespagram (model) back-azimuths of -94 ± 14 (-95 ± 16), -21 ± 14 (-15 ± 8) and 26 ± 6 (34 ± 7).

A similarity index (SI), taken from an imaging processing approach, is introduced as

$$\mathrm{SI}(t) = 1 - \mathrm{MSE}(t) = \frac{1}{N_\theta} \sum_{\theta} \left[P_{\text{model}}(t,\theta) - P_{\text{vespa}}(t,\theta) \right]^2, \tag{3}$$

where MSE is a mean squared error between normalized smoothed model output, $P_{\text{model}}(t,\theta)$, and normalized vespagram, $P_{\text{vespa}}(t,\theta)$, calculated at each time step, θ is back-azimuth, t is time. The use of normalized data is justified by the influence of the smoothing procedure on the magnitude of the model data. MSE provides information on how accurate the model reproduces the directional pressure spectrum (zero indicates full match between model and infrasound vespagram). Panel h) in Figures 2 and 3 presents values of SI obtained over a year.

In winter, SI for lower frequencies is stable and has values ~ 1, with exceptions corresponding to increased noise level in vespagrams or to SSW events that are discussed below. Relatively low SI for higher frequencies can be explained either by spurious apparent sources corresponding to array response function side-lobes (Figure 1b) or by presence of sources in the vespagram that are missed or not-well reproduced in the model because of a 5000 km distance limit (see Sect. 2.2). In summer, SI values are quite variable and unstable but never fall below 0.5. Such behavior is typical regardless of year and frequency band (Figure 5). One possible explanation is the changing weather conditions present at the station throughout the year. For example, Orsolini and Sorteberg (2009) have shown an enhancement in the number and intensity of summer cyclones the Arctic and Northern Eurasia. This would result in additional wind and rain noise in the infrasound recordings that would especially be enhanced at the lower frequencies. Another possible contribution would be the poor resolution of the array at low frequencies that can mix stratospheric signals with those from higher altitudes. These sometimes dominate at IS37 in summer (Näsholm et al., 2020) but are not included in the model. The relative stability of the model's results in Figure 3 relative to the vespagram would indicate that there are additional sources of variability, either atmospheric, source region, or propagation path, that are not well characterized in the model.

As indicated by the high SI values, especially in winter, the infrasound data processed in the framework of vespa approach are in a good agreement with modelled microbarom soundscapes in both time (seasonal variations) and space (directional distribution). The similarity estimation proposed allows detection of inconsistencies between the microbarom model and the vespa processing which might be used for identifying biases in atmospheric models. This is especially promisingly for low frequencies where side-lobes of array response do not appreciably affect analysis.

3.2 Examination of major sudden stratospheric warmings

Although this is not the main objective of the current study, in this section we examine the ability of the vespagrams to detect extreme atmospheric events, such as sudden stratospheric warmings (SSWs), and compare model and vespa processing for six selected events.

https://doi.org/10.5194/angeo-2020-78
Preprint. Discussion started: 8 December 2020

Annales Geophysicae Discussions
Open Access
EGU

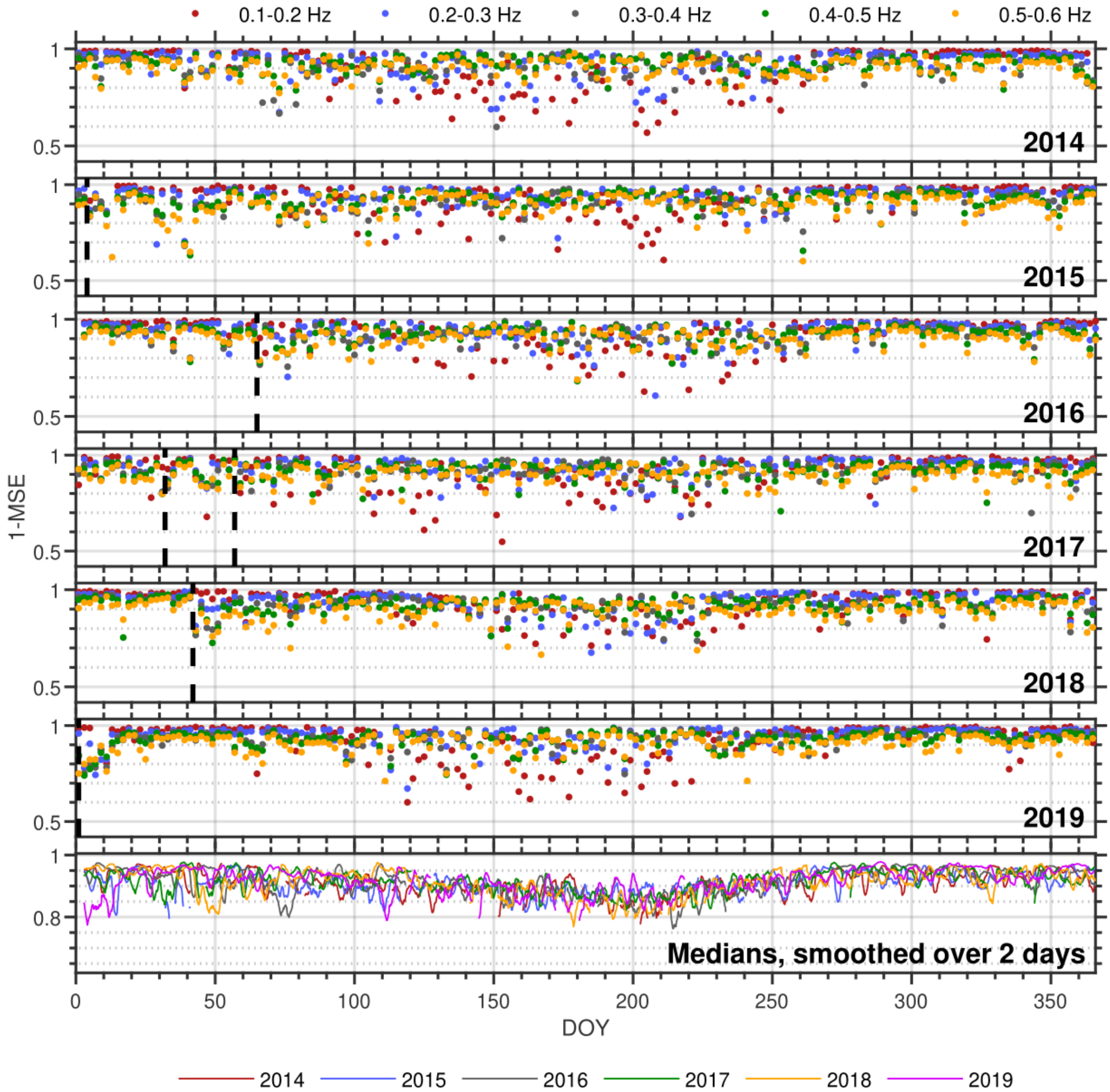

Figure 5. Multi-year comparison between modelled microbarom soundscapes at the IS37 station after smoothing and vespagrams. The similarity index is color-coded depending on frequency band: 0.1 – 0.2 Hz – red, 0.2 – 0.3 Hz – blue, 0.3 – 0.4 Hz – grey, 0.4 – 0.5 Hz – green, 0.5 – 0.6 Hz – orange. Data are presented with 3 days interval. Black dashed lines present SSWs onsets. Medians over frequency bands in the last panel are color-coded depending on year: 2014 – red, 2015 – blue, 2016 – grey, 2017 – green, 2018 – yellow, 2019 – magenta.

SSWs usually occur in wintertime and are, in general, associated with a sudden and short increase in stratospheric temperature and mesospheric cooling at high / middle latitudes (Shepherd et al., 2014; Butler et al., 2015; Limpasuvan et al., 2016; Zülicke et al., 2018). SSWs are often classified into minor and major warmings, depending on whether there was a weakening or reversal of the zonal wind (Butler et al., 2015). During the period of our consideration, three major and three minor SSWs occurred. Major SSWs took place with onsets on 5-6 March 2016 (Manney and Lawrence, 2016), 11 February 2018 (Rao et al., 2018; Lü et al., 2020) and 1 January 2019 (Rao et al., 2019, 2020), while the minor events occurred with onsets on 4 January 2015 (Manney et al., 2015; Mitnik et al., 2018), 1 and 26 February 2017 (Eswaraiah et al., 2020). Note that there can be an error up to several days in determining SSW onset day since there is no single way to define the onset, and different authors use different definitions. A prime example is the first SSW in 2017. According to the definition of the World Meteorological Organization, this event is classified as minor, but in a number of studies it is referred to as major (Xiong et al., 2018; Conte et al., 2019). Vertical dashed lines in Figures 5 – 6 correspond to the onset days listed above when SSW criteria were met.

The infrasound signature reported by Donn and Rind (1971) and Evers and Siegmund (2009), which showed a significant change in direction of the infrasound arrival due to a change in favorable stratospheric waveguide, can be seen in Figure 6 for all SSWs under consideration and in Figures 2 and 3 e) - j) for the 2016 SSW. The change in direction from the North Atlantic to the Barents Sea is clearly pronounced in both model and vespagrams around SSWs onset days. Figure 2 f) – j) demonstrates that the signature appears late in the model data and its duration is much shorter than in vespagram, analogous to study by Smets et al. (2016). For higher frequencies (Figure 3) the duration of a change from eastward to westward pattern is longer and continues until late March – early April that corresponds to reanalysis data (Manney and Lawrence, 2016).

Another feature revealed is a significant decrease in similarity index between model and observations during SSWs (Figure 5) which is characteristic for all events under consideration. The smallest discrepancies in the direction of the dominant wave front between the model and infrasound data during SSWs reach about $5° - 7°$, but the largest reach as much as $90° - 100°$ (Figure 6). This may be caused by the following factors. The back-azimuth change during SSW usually appears earlier in the vespagrams than in the model with the difference of 3 to 24 hours. Similar results were previously obtained by Smets and Evers (2014) and can be explained by the presence of an error in determining SSW onset day from reanalysis data because of a scarcity of observations at stratospheric altitudes (Charlton-Perez et al., 2013) or by inadequate stratospheric analysis and forecast during SSWs as addressed by (Diamantakis, 2014; Smets et al., 2016). Sometimes the SSW signature does not appear in the vespagrams while appearing in the model (see Figure 6 around SSW 2018 onset day for example). This can arise when employing a horizontally homogeneous atmosphere and overly constraining the model with the ECMWF wind and temperature at 50 km altitude. Such approach does not allow a full, altitude dependent description of infrasonic waves in the atmosphere and causes discrepancies between model and vespagrams. Considering long propagation path for microbaroms, net wind effect along the propagation path can be equal to zero in vespagram in contrast to the model, which estimates the probability of signal arrival at the final point of the path. It has been demonstrated by (Evers and Siegmund, 2009; Smets and Evers, 2014) that ECMWF wind direction not always characterize the actual infrasound path, resulting is model-vespagram discrepancies.

Despite slight difference in the dominant direction of wave front arrival during SSW, both model and vespagrams reproduce changes in infrasound pattern correctly in time. Moreover, since vespagrams can detect changes in stratospheric dynamics during extreme events, there is a potential in using it in near-real-time stratospheric diagnostics.

https://doi.org/10.5194/angeo-2020-78
Preprint. Discussion started: 8 December 2020

Annales Geophysicae Discussions

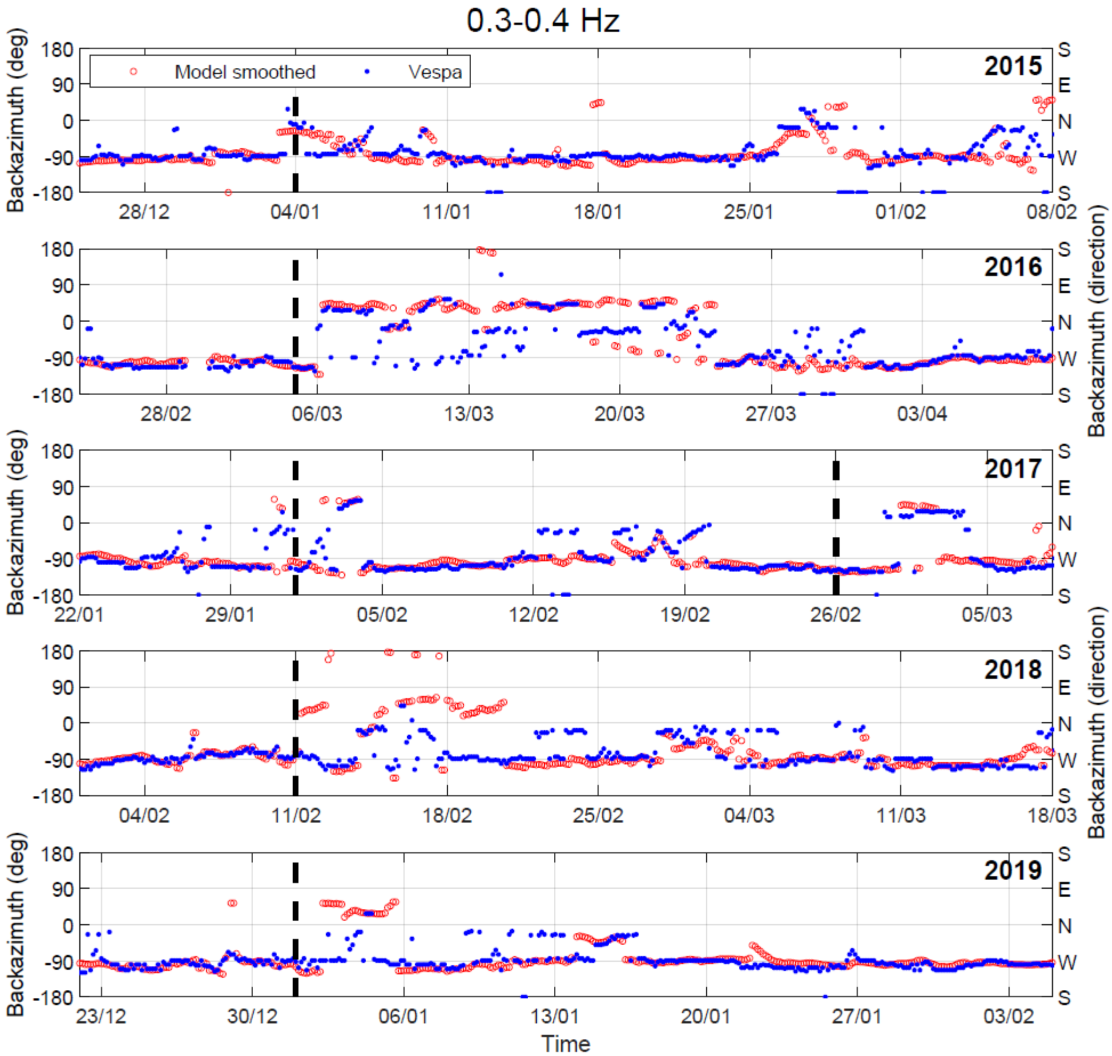

Figure 6. Changes in the backazimuth direction of the dominant wave front as recorded and modelled for the IS37 station (blue – vespagram from infrasound data, red – microbarom model, smoothed) around SSWs 2015 – 2019 for the 0.3 – 0.4 Hz band. Black dashed lines indicate days when SSWs (minor or major) criteria were met.

4 Discussion and Conclusions

In this study, we compare observed and predicted microbaroms soundscapes using a vespagram-based approach. Analysis is performed based on calculation of microbaroms power as a function of time and back-azimuth at constant apparent velocity of 350 m/s. Note, however, that the vespagram-family of time-dependent microbarom data visualizations can be constructed also using other array processing techniques that estimate power as function of the slowness of the wave front, e.g., using robust estimators as explored by Bishop et al. (2020), or adaptive high-resolution approaches like Capon's method (Capon, 1969).

An advantage of the vespagram-approach is that microbarom radiation and propagation models can be benchmarked against recorded infrasound data for all directions simultaneously, as opposed to methods where only the back-azimuth direction of maximum power is considered (e.g., Hupe et al., 2019; Smirnov et al., 2020). Since the vespa processing is computationally low-cost and able to track variations in microbarom parameters over extended periods spanning one or several years, it can be utilized for near-real time assessment of atmospheric model products and for developing infrasound-based stratospheric diagnostics. It can also be used when assessing changes in infrasound signatures over shorter time windows, e.g., during extreme atmospheric events.

Limitations in this study are predominantly related to microbarom propagation modelling. In addition to the scarcity of observations at the stratospheric altitudes (Charlton-Perez et al., 2013) which affect the accuracy of directional distribution of predicted microbarom soundscapes, the horizontally homogeneous atmospheric approximation used in the study creates substantial limitations. These are especially pronounced for long-distance propagation when infrasound waves pass through several atmospheric regions which disturb the wind on smaller scales, such as tidal phases or SSW events. Moreover, the modelling would benefit from applying a full-waveform simulation code for the propagation of the radiated microbaroms to the station (e.g., Assink et al., 2014; Kim and Rodgers, 2017; Brissaud et al., 2017; Petersson and Sjögreen, 2018; Sabatini et al., 2019). This would provide a more refined modelling of the atmospheric ducting compared to the semi-empirical approach (Le Pichon et al., 2012) applied in the current study. An alternative which is less computational expensive is (3-D) ray-tracing, which can account for both range-dependent atmospheric models and cross-wind effects (e.g., Smets and Evers, 2014; Smets et al., 2016). However, the inherent high-frequency approximation of the ray-theory can limit the modelling of diffraction and scattering effects (Chunchuzov et al., 2015) that can be important for the low-frequency microbaroms.

A more elaborate microbarom propagation model could also allow for an estimate of the full microbarom wavefield impinging an infrasound station, hence providing an estimate of its power within the full horizontal slowness space of plane wave front directions (or a selected relevant region). This way, we could benchmark the modelled and recorded microbarom field at an infrasound array for each sliding time window without restricting the analysis to the region around a fixed apparent velocity as carried out in the current study. Notably, such "f-k plots" of modelled and recorded microbaroms are also (time-varying) images which can be assessed and compared using the versatile ecosystem of image processing and image comparison algorithms.

Future developments can include compilation of long-term time-dependent statistics of similarity between model and infrasound recordings for multiple stations on global and regional scales, in order to define anomaly flag criteria which would indicate that there is unexpected inconsistency between model and observations due to, for example, biases in atmospheric model products. Moreover, we suggest to apply the presented approach in global assessment and comparisons of ocean wave-action model products, as well as in validation and further refinement of microbarom radiation estimation algorithms.

Author contributions. EV and SPN developed the vespagram calculation code, performed the infrasound data processing, and made the model/data analysis. MDC and ALP developed the microbarom model code and performed the simulations. EV prepared the manuscript with contributions from all co-authors. SPN and ALP initiated the study.

Competing interests. The authors declare that they have no conflict of interest.

Acknowledgements. This study was facilitated by previous research performed within the framework of the ARISE and ARISE2 projects (Blanc et al., 2018, 2019), funded by the European Commission FP7 and Horizon 2020 programmes (Grant agreements 284387 and 653980). EV and SPN are grateful to Y. J. Orsolini for discussion and valuable comments. The vespagram and microbarom model images are visualized using the Turbo colormap (Mikhailov, 2019).

Financial support. This research was supported by the Research Council of Norway FRIPRO/FRINATEK basic research programme, project contract 274377: *Middle Atmosphere Dynamics: Exploiting Infrasound Using a Multidisciplinary Approach at High Latitudes* (MADEIRA).

https://doi.org/10.5194/angeo-2020-78
Preprint. Discussion started: 8 December 2020

Annales Geophysicae
Discussions

References

Amezcua, J., Näsholm, S. P., Blixt, E. M., and Charlton-Perez, A. J.: Assimilation of atmospheric infrasound data to constrain tropospheric and stratospheric winds, Quarterly Journal of the Royal Meteorological Society, 2020.

Ardhuin, F., Stutzmann, E., Schimmel, M., and Mangeney, A.: Ocean wave sources of seismic noise, Journal of Geophysical Research: Oceans, 116, 2011.

Assink, J., Pichon, A. L., Blanc, E., Kallel, M., and Khemiri, L.: Evaluation of wind and temperature profiles from ECMWF analysis on two hemispheres using volcanic infrasound, Journal of Geophysical Research: Atmospheres, 119, 8659–8683, 2014.

Assink, J., Smets, P., Marcillo, O., Weemstra, C., Lalande, J.-M., Waxler, R., and Evers, L.: Advances in infrasonic remote sensing methods, in: Infrasound Monitoring for Atmospheric Studies, pp. 605–632, Springer, 2019.

Baird, H. and Banwell, C.: Recording of air-pressure oscillations associated with microseisms at Christchurch, NZJ Sci. Technol., Sect. B, 21, 314–329, 1940.

Benioff, H. and Gutenberg, B.: Waves and currents recorded by electromagnetic barographs, Bulletin of the American Meteorological Society, 20, 421–428, 1939.

Bishop, J. W., Fee, D., and Szuberla, C. A. L.: Improved infrasound array processing with robust estimators, Geophysical Journal International, 221, 2058–2074, https://doi.org/10.1093/gji/ggaa110, 2020.

Blanc, E., Ceranna, L., Hauchecorne, A., Charlton-Perez, A., Marchetti, E., Evers, L., Kvaerna, T., Lastovicka, J., Eliasson, L., Crosby, N., Blanc-Benon, P., Le Pichon, A., Brachet, N., Pilger, C., Keckhut, P., Assink, J., Smets, P. M., Lee, C., Kero, J., Sindelarova, T., Kämpfer, N., Rüfenacht, R., Farges, T., Millet, C., Näsholm, S., Gibbons, S., Espy, P., Hibbins, R., Heinrich, P., Ripepe, M., Khaykin, S., Mze, N., and Chum, J.: Toward an Improved Representation of Middle Atmospheric Dynamics Thanks to the ARISE Project, Surveys in Geophysics, 39, 171–225, https://doi.org/10.1007/s10712-017-9444-0, 2018.

Blanc, E., Pol, K., Le Pichon, A., Hauchecorne, A., Keckhut, P., Baumgarten, G., Hildebrand, J., Höffner, J., Stober, G., Hibbins, R., Espy, P., Rapp, M., Kaifler, B., Ceranna, L., Hupe, P., Hagen, J., Rüfenacht, R., Kämpfer, N., and Smets, P.: Middle atmosphere variability and model uncertainties as investigated in the framework of the ARISE project, in: Infrasound Monitoring for Atmospheric Studies, pp. 845–887, Springer, 2019.

Brekhovskikh, L., Goncharov, V., Kurtepov, V., and KA, N.: Radiation of infrasound into atmosphere by surface-waves in ocean, Izvestiya Akademii Nauk SSSR Fizika Atmosfery i Okeana, 9, 899–907, 1973.

Brissaud, Q., Martin, R., Garcia, R. F., and Komatitsch, D.: Hybrid Galerkin numerical modelling of elastodynamics and compressible Navier–Stokes couplings: applications to seismo-gravito acoustic waves, Geophysical Journal International, 210, 1047–1069, 2017.

Büeler, D., Beerli, R., Wernli, H., and Grams, C. M.: Stratospheric influence on ECMWF sub-seasonal forecast skill for energy-industry-relevant surface weather in European countries, Quarterly Journal of the Royal Meteorological Society, 2020.

Butler, A. H., Seidel, D. J., Hardiman, S. C., Butchart, N., Birner, T., and Match, A.: Defining sudden stratospheric warmings, Bulletin of the American Meteorological Society, 96, 1913–1928, 2015.

Capon, J.: High-resolution frequency-wavenumber spectrum analysis, Proceedings of the IEEE, 57, 1408–1418, 1969.

Charlton-Perez, A. J., Baldwin, M. P., Birner, T., Black, R. X., Butler, A. H., Calvo, N., Davis, N. A., Gerber, E. P., Gillett, N., Hardiman, S., Kim, J., Krüger, K., Lee, Y.-Y., Manzini, E., McDaniel, B. A., Polvani, L., Reichler, T., Shaw, T. A., Sigmond, M., Son, S.-W., Toohey, M., Wilcox, L., Yoden, S., Christiansen, B., Lott, F., Shindell, D., Yukimoto, S., and Watanabe, S.: On the lack of stratospheric dynamical variability in low-top versions of the CMIP5 models, Journal of Geophysical Research: Atmospheres, 118, 2494–2505, 2013.

Chunchuzov, I., Kulichkov, S., Perepelkin, V., Popov, O., Firstov, P., Assink, J., and Marchetti, E.: Study of the wind velocity-layered structure in the stratosphere, mesosphere, and lower thermosphere by using infrasound probing of the atmosphere, Journal of Geophysical Research: Atmospheres, 120, 8828–8840, 2015.

Conte, J. F., Chau, J. L., and Peters, D. H.: Middle-and High-Latitude Mesosphere and Lower Thermosphere Mean Winds and Tides in Response to Strong Polar-Night Jet Oscillations, Journal of Geophysical Research: Atmospheres, 124, 9262–9276, 2019.

Dahlman, O., Mykkeltveit, S., and Haak, H.: Nuclear test ban: converting political visions to reality, Springer Science & Business Media, 2009.

Davies, D., Kelly, E., and Filson, J.: Vespa process for analysis of seismic signals, Nature Physical Science, 232, 8–13, 1971.

De Carlo, M., Le Pichon, A., Vergoz, J., Ardhuin, F., Näsholm, S., Ceranna, L., Hupe, P., and Pilger, C.: Characterizing ocean ambient noise in the North Atlantics and the Barents Sea regions, in: CTBTO Infrasound Technology Workshop (ITW), 2019.

De Carlo, M., Ardhuin, F., Ceranna, L., Hupe, P., Le Pichon, A., and Vergoz, J.: Global comparison between ocean ambient noise modelling and infrasound network observations, in: EGU General Assembly Conference Abstracts, p. 17475, https://doi.org/10.5194/egusphere-egu2020-17475, 2020.

De Carlo, M., Ardhuin, F., and Le Pichon, A.: Atmospheric infrasound generation by ocean waves in finite depth: unified theory and application to radiation patterns, Geophysical Journal International, 221, 569–585, https://doi.org/10.1093/gji/ggaa015, 2020.

den Ouden, O. F. C., Assink, J. D., Smets, P. S. M., Shani-Kadmiel, S., Averbuch, G., and Evers, L. G.: CLEAN beamforming for the enhanced detection of multiple infrasonic sources, Geophysical Journal International, 221, 305–317, 2020.

Dessauer, F., Graffunder, W., and Schaffhauser, J.: Über atmosphärische Pulsationen, Archiv für Meteorologie, Geophysik und Bioklimatologie, Serie A, 3, 453–463, 1951.

Diamantakis, M.: Improving ECMWF forecasts of sudden stratospheric warmings, ECMWF Newsletter, 141, 30–36, 2014.

Domeisen, D. I. V., Butler, A. H., Charlton-Perez, A. J., Ayarzagüena, B., Baldwin, M. P., Dunn-Sigouin, E., Furtado, J. C., Garfinkel, C. I., Hitchcock, P., Karpechko, A. Y., Kim, H., Knight, J., Lang, A. L., Lim, E.-P., Marshall, A., Roff, G., Schwartz, C., Simpson, I. R., Son, S.-W., and Taguchi, M.: The Role of the Stratosphere in Subseasonal to Seasonal Prediction: 1. Predictability of the Stratosphere, Journal of Geophysical Research: Atmospheres, 125, e2019JD030 920, 2020a.

Domeisen, D. I. V., Butler, A. H., Charlton-Perez, A. J., Ayarzagüena, B., Baldwin, M. P., Dunn-Sigouin, E., Furtado, J. C., Garfinkel, C. I., Hitchcock, P., Karpechko, A. Y., Kim, H., Knight, J., Lang, A. L., Lim, E.-P., Marshall, A., Roff, G., Schwartz, C., Simpson, I. R., Son, S.-W., and Taguchi, M.: The Role of the Stratosphere in Subseasonal to Seasonal Prediction: 2. Predictability Arising From Stratosphere-Troposphere Coupling, Journal of Geophysical Research: Atmospheres, 125, e2019JD030 923, 2020b.

Donn, W. L. and Posmentier, E. S.: Infrasonic waves from the marine storm of April 7, 1966, Journal of Geophysical Research, 72, 2053–2061, 1967.

Donn, W. L. and Rind, D.: Natural infrasound as an atmospheric probe, Geophysical Journal International, 26, 111–133, 1971.

Dorrington, J., Finney, I., Palmer, T., and Weisheimer, A.: Beyond skill scores: exploring sub-seasonal forecast value through a case study of French month-ahead energy prediction, Quarterly Journal of the Royal Meteorological Society, 2020.

Eswaraiah, S., Kumar, K. N., Kim, Y. H., Chalapathi, G. V., Lee, W., Jiang, G., Yan, C., Yang, G., Ratnam, M. V., Prasanth, P. V., et al.: Low-latitude mesospheric signatures observed during the 2017 sudden stratospheric warming using the fuke meteor radar and ERA-5, Journal of Atmospheric and Solar-Terrestrial Physics, p. 105352, 2020.

Evers, L. and Siegmund, P.: Infrasonic signature of the 2009 major sudden stratospheric warming, Geophysical Research Letters, 36, 2009.

Fyen, J., Roth, M., and W., L. P.: IS37 Infrasound Station in Bardufoss, Norway, NORSAR Scientific Report, p. 29–39, 2014.

Garcés, M., Hansen, R. A., and Lindquist, K. G.: Traveltimes for infrasonic waves propagating in a stratified atmosphere, Geophysical journal international, 135, 255–263, 1998.

Garcés, M., Willis, M., Hetzer, C., Le Pichon, A., and Drob, D.: On using ocean swells for continuous infrasonic measurements of winds and temperature in the lower, middle, and upper atmosphere, Geophysical research letters, 31, 2004.

Gibbons, S., Ringdal, F., and Kværna, T.: Joint seismic-infrasonic processing of recordings from a repeating source of atmospheric explosions, The Journal of the Acoustical Society of America, 122, EL158–EL164, 2007.

Gibbons, S., Asming, V., Eliasson, L., Fedorov, A., Fyen, J., Kero, J., Kozlovskaya, E., Kværna, T., Liszka, L., Näsholm, P., Raita, T., Roth, M., Tiira, T., and Vinogradov, Y.: The European Arctic: A Laboratory for Seismoacoustic Studies, Seismological Research Letters, 86, 917–928, https://doi.org/10.1785/0220140230, 2015.

Gibbons, S., Kværna, T., and Näsholm, S.: Characterization of the infrasonic wavefield from repeating seismo-acoustic events, in: Infrasound Monitoring for Atmospheric Studies, pp. 387–407, Springer, 2019.

Gibbons, S. J., Kværna, T., Tiira, T., and Kozlovskaya, E.: A Benchmark Case Study for Seismic Event Relative Location, Geophysical Journal International, https://doi.org/10.1093/gji/ggaa362, 2020.

Gutenberg, B. and Benioff, H.: Atmospheric-pressure waves near Pasadena, Eos, Transactions American Geophysical Union, 22, 424–426, 1941.

Hasselmann, K.: A statistical analysis of the generation of microseisms, Reviews of Geophysics, 1, 177–210, 1963.

Hibbins, R., Espy, P., and de Wit, R.: Gravity-Wave Detection in the Mesosphere Using Airglow Spectrometers and Meteor Radars, in: Infrasound Monitoring for Atmospheric Studies, pp. 649–668, Springer, 2019.

Hillers, G., Graham, N., Campillo, M., Kedar, S., Landès, M., and Shapiro, N.: Global oceanic microseism sources as seen by seismic arrays and predicted by wave action models, Geochemistry, Geophysics, Geosystems, 13, 2012.

Högbom, J. A.: Aperture synthesis with a non-regular distribution of interferometer baselines, Astronomy and Astrophysics Supplement Series, 15, 417, 1974.

Hupe, P., Ceranna, L., Pilger, C., De Carlo, M., Le Pichon, A., Kaifler, B., and Rapp, M.: Assessing middle atmosphere weather models using infrasound detections from microbaroms, Geophysical Journal International, 216, 1761–1767, 2019.

Ingate, S., Husebye, E., and Christoffersson, A.: Regional arrays and optimum data processing schemes, Bulletin of the Seismological Society of America, 75, 1155–1177, 1985.

Kanasewich, E., Hemmings, C., and Alpaslan, T.: Nth-root stack nonlinear multichannel filter, Geophysics, 38, 327–338, 1973.

Kim, K. and Rodgers, A.: Influence of low-altitude meteorological conditions on local infrasound propagation investigated by 3-D full-waveform modeling, Geophysical Journal International, 210, 1252–1263, 2017.

Landès, M., Le Pichon, A., Shapiro, N. M., Hillers, G., and Campillo, M.: Explaining global patterns of microbarom observations with wave action models, Geophysical Journal International, 199, 1328–1337, 2014.

Le Pichon, A., Ceranna, L., Garcés, M., Drob, D., and Millet, C.: On using infrasound from interacting ocean swells for global continuous measurements of winds and temperature in the stratosphere, Journal of Geophysical Research: Atmospheres, 111, 2006.

Le Pichon, A., Vergoz, J., Herry, P., and Ceranna, L.: Analyzing the detection capability of infrasound arrays in Central Europe, Journal of Geophysical Research: Atmospheres, 113, 2008.

Le Pichon, A., Ceranna, L., and Vergoz, J.: Incorporating numerical modeling into estimates of the detection capability of the IMS infrasound network, Journal of Geophysical Research: Atmospheres, 117, 1–12, https://doi.org/10.1029/2011JD016670, https://agupubs.onlinelibrary.wiley.com/doi/abs/10.1029/2011JD016670, 2012.

Le Pichon, A., Assink, J. D., Heinrich, P., Blanc, E., Charlton-Perez, A., Lee, C. F., Keckhut, P., Hauchecorne, A., Rüfenacht, R., Kämpfer, N., Drob, D. P., Smets, P. S. M., Evers, L. G., Ceranna, L., Pilger, C., Ross, O., and Claud, C.: Comparison of co-located independent ground-based middle atmospheric wind and temperature measurements with numerical weather prediction models, Journal of Geophysical Research: Atmospheres, 120, 8318–8331, 2015.

Le Pichon, A., Ceranna, L., Vergoz, J., and Tailpied, D.: Modeling the detection capability of the global IMS infrasound network, in: Infrasound Monitoring for Atmospheric Studies, pp. 593–604, Springer, 2019.

Limpasuvan, V., Orsolini, Y. J., Chandran, A., Garcia, R. R., and Smith, A. K.: On the composite response of the MLT to major sudden stratospheric warming events with elevated stratopause, Journal of Geophysical Research: Atmospheres, 121, 4518–4537, https://doi.org/10.1002/2015JD024401, 2016.

Lonzaga, J. B.: A theoretical relation between the celerity and trace velocity of infrasonic phases, The Journal of the Acoustical Society of America, 138, EL242–EL247, 2015.

Lü, Z., Li, F., Orsolini, Y. J., Gao, Y., and He, S.: Understanding of european cold extremes, sudden stratospheric warming, and siberian snow accumulation in the winter of 2017/18, Journal of Climate, 33, 527–545, 2020.

Manney, G. L. and Lawrence, Z. D.: The major stratospheric final warming in 2016: Dispersal of vortex air and termination of Arctic chemical ozone loss, Atmospheric Chemistry & Physics, 16, 2016.

Manney, G. L., Lawrence, Z. D., Santee, M. L., Read, W. G., Livesey, N. J., Lambert, A., Froidevaux, L., Pumphrey, H. C., and Schwartz, M. J.: A minor sudden stratospheric warming with a major impact: Transport and polar processing in the 2014/2015 Arctic winter, Geophysical Research Letters, 42, 7808–7816, 2015.

Marty, J.: The IMS infrasound network: current status and technological developments, in: Infrasound Monitoring for Atmospheric Studies, pp. 3–62, Springer, 2019.

McFadden, P., Drummond, B., and Kravis, S.: The N th-root stack: Theory, applications, and examples, Geophysics, 51, 1879–1892, 1986.

Mikhailov, A.: Turbo, An Improved Rainbow Colormap for Visualization, https://ai.googleblog.com/2019/08/turbo-improved-rainbow-colormap-for.html, accessed: 25 July 2020, 2019.

Mitnik, L. M., Kuleshov, V., Pichugin, M. K., and Mitnik, M. L.: Sudden Stratospheric Warming in 2015–2016: Study with Satellite Passive Microwave Data and ERA5 Reanalysis, in: IGARSS 2018-2018 IEEE International Geoscience and Remote Sensing Symposium, pp. 5556–5559, IEEE, 2018.

Muirhead, K. and Datt, R.: The N-th root process applied to seismic array data, Geophysical Journal International, 47, 197–210, 1976.

Näsholm, S. P., Vorobeva, E., Le Pichon, A., Orsolini, Y. J., Turquet, A. L., Hibbins, R. E., Espy, P. J., De Carlo, M., Assink, J. D., and Rodriguez, I. V.: Semidiurnal tidal signatures in microbarom infrasound array measurements, in: EGU General Assembly Conference Abstracts, p. 19035, 2020.

Nippress, A., Green, D. N., Marcillo, O. E., and Arrowsmith, S. J.: Generating regional infrasound celerity-range models using ground-truth information and the implications for event location, Geophysical Journal International, 197, 1154–1165, 2014.

Orsolini, Y. J. and Sorteberg, A.: Projected changes in Eurasian and Arctic summer cyclones under global warming in the Bergen climate model, Atmospheric and Oceanic Science Letters, 2, 62–67, 2009.

Petersson, N. A. and Sjögreen, B.: High order accurate finite difference modeling of seismo-acoustic wave propagation in a moving atmosphere and a heterogeneous earth model coupled across a realistic topography, Journal of Scientific Computing, 74, 290–323, 2018.

https://doi.org/10.5194/angeo-2020-78
Preprint. Discussion started: 8 December 2020

Annales Geophysicae Discussions

Pilger, C., Ceranna, L., Ross, J. O., Vergoz, J., Le Pichon, A., Brachet, N., Blanc, E., Kero, J., Liszka, L., Gibbons, S., Kvaerna, T., Näsholm, S. P., Marchetti, E., Ripepe, M., Smets, P., Evers, L., Ghica, D., Ionescu, C., Sindelarova, T., Ben Horin, Y., and Mialle, P.: The European Infrasound Bulletin, Pure and Applied Geophysics, 175, 3619–3638, 2018.

Pilger, C., Gaebler, P., Ceranna, L., Le Pichon, A., Vergoz, J., Perttu, A., Tailpied, D., and Taisne, B.: Infrasound and seismoacoustic signatures of the 28 September 2018 Sulawesi super-shear earthquake, Natural Hazards and Earth System Sciences, 19, 2811–2825, https://doi.org/10.5194/nhess-19-2811-2019, https://nhess.copernicus.org/articles/19/2811/2019/, 2019.

Polavarapu, S., Shepherd, T., Rochon, Y., and Ren, S.: Some challenges of middle atmosphere data assimilation, Quarterly Journal of the Royal Meteorological Society: A journal of the atmospheric sciences, applied meteorology and physical oceanography, 131, 3513–3527, 2005.

Rao, J., Ren, R., Chen, H., Yu, Y., and Zhou, Y.: The stratospheric sudden warming event in February 2018 and its prediction by a climate system model, Journal of Geophysical Research: Atmospheres, 123, 13–332, 2018.

Rao, J., Garfinkel, C. I., Chen, H., and White, I. P.: The 2019 New Year stratospheric sudden warming and its real-time predictions in multiple S2S models, Journal of Geophysical Research: Atmospheres, 124, 11 155–11 174, 2019.

Rao, J., Garfinkel, C. I., and White, I. P.: Predicting the downward and surface influence of the February 2018 and January 2019 sudden stratospheric warming events in subseasonal to seasonal (S2S) models, Journal of Geophysical Research: Atmospheres, 125, e2019JD031 919, 2020.

Rienecker, M. M., Suarez, M. J., Gelaro, R., Todling, R., Bacmeister, J., Liu, E., Bosilovich, M. G., Schubert, S. D., Takacs, L., Kim, G.-K., Bloom, S., Chen, J., Collins, D., Conaty, A., da Silva, A., Gu, W., Joiner, J., Koster, R. D., Lucchesi, R., Molod, A., Owens, T., Pawson, S., Pegion, P., Redder, C. R., Reichle, R., Robertson, F. R., Ruddick, A. G., Sienkiewicz, M., and Woollen, J.: MERRA: NASA's modern-era retrospective analysis for research and applications, Journal of climate, 24, 3624–3648, 2011.

Rost, S. and Thomas, C.: Array seismology: Methods and applications, Reviews of geophysics, 40, 2–1, 2002.

Sabatini, R., Marsden, O., Bailly, C., and Gainville, O.: Three-dimensional direct numerical simulation of infrasound propagation in the Earth's atmosphere, Journal of Fluid Mechanics, 859, 754–789, 2019.

Saxer, L.: Elektrische messung kleiner atmospharischer druckschwankungen, HELVETICA PHYSICA ACTA, 18, 527–550, 1945.

Saxer, L.: Über Entstehung und Ausbreitung quasiperiodischer Luftdruckschwankungen, Archiv für Meteorologie, Geophysik und Bioklimatologie, Serie A, 6, 451–463, 1954.

Shepherd, M. G., Beagley, S. R., and Fomichev, V. I.: Stratospheric warming influence on the mesosphere/lower thermosphere as seen by the extended CMAM, Annales Geophysicae, 32, 589–608, https://doi.org/10.5194/angeo-32-589-2014, 2014.

Smets, P. and Evers, L.: The life cycle of a sudden stratospheric warming from infrasonic ambient noise observations, Journal of Geophysical Research: Atmospheres, 119, 12–084, 2014.

Smets, P., Assink, J., Le Pichon, A., and Evers, L.: ECMWF SSW forecast evaluation using infrasound, Journal of Geophysical Research: Atmospheres, 121, 4637–4650, 2016.

Smets, P., Assink, J., and Evers, L.: The study of sudden stratospheric warmings using infrasound, in: Infrasound Monitoring for Atmospheric Studies, pp. 723–755, Springer, 2019.

Smirnov, A., De Carlo, M., Le Pichon, A., Shapiro, N. M., and Kulichkov, S.: Characterizing the global ocean ambient noise as recorded by the dense seismo-acoustic Kazakh network, Solid Earth Discussions, 2020, 1–25, https://doi.org/10.5194/se-2020-8, 2020.

Smith, A. K.: Global dynamics of the MLT, Surveys in Geophysics, 33, 1177–1230, 2012.

Waxler, R., Gilbert, K., Talmadge, C., and Hetzer, C.: The effects of the finite depth of the ocean on microbarom signals, in: 8th International Conference on Theoretical and Computational Acoustics (ICTCA), Crete, Greece, 2007.

https://doi.org/10.5194/angeo-2020-78
Preprint. Discussion started: 8 December 2020

Whitaker, R. W. and Mutschlecner, J. P.: A comparison of infrasound signals refracted from stratospheric and thermospheric altitudes, Journal of Geophysical Research: Atmospheres, 113, 2008.

Xiong, J., Wan, W., Ding, F., Liu, L., Hu, L., and Yan, C.: Two day wave traveling westward with wave number 1 during the sudden stratospheric warming in January 2017, Journal of Geophysical Research: Space Physics, 123, 3005–3013, 2018.

Zülicke, C., Becker, E., Matthias, V., Peters, D. H., Schmidt, H., Liu, H.-L., Ramos, L. d. l. T., and Mitchell, D. M.: Coupling of stratospheric warmings with mesospheric coolings in observations and simulations, Journal of Climate, 31, 1107–1133, 2018.